A Robust Spectroscopic Method for the Determination of Protein Conformational Composition- Application to the Annealing of Silk

David J. Belton[1], **Robyn Plowright**[1], **David L. Kaplan**[2], and **Carole C. Perry**[1,*]

[1]Interdisciplinary Biomedical Research Centre, Nottingham Trent University, Clifton Lane, Nottingham NG11 8NS

[2]Department of Biomedical Engineering, Tufts University, Medford, MA, 02155, USA

Abstract

The physical and mechanical properties of structural proteins such as silk fibroin can be modified by controlled conformational change, which is regularly monitored by Fourier transform infrared spectroscopy by peak fitting of the amide I band envelope. Although many variables affecting peak shape are well established, there is no fixed methodology to compare and follow secondary structural differences without significant operator input especially where low frequency spectral noise is a problem.

The aim of this contribution is to establish a method for such analyses to be carried at high levels of autonomy to prevent subjective or erroneous fitting. A range of approaches was trialled with optimal peak parameters selected based on overall goodness of fit and reproducibility of fit of replicate sample spectra. The method was successfully tested against reference proteins having contrasting β content and the rationale for parameter selection is presented.

Further, we applied this method to measure the effect of conformational change on the energy of the amide I band of silk fibroin during annealing. Energy changes were ca. 400 KJmol^{-1} of fibroin. To confirm that this energy change was a consequence of increased hydrogen bonding we used a Thioflavin T staining method typically used to identify β aggregate type structures in amyloid plaques.
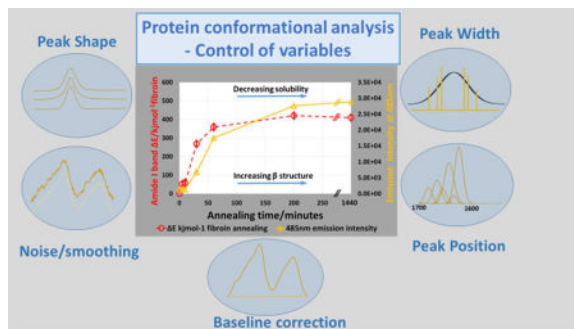
We propose that the approach described herein can aid in the development of silk based materials for biomedical applications where tuning of the physical and mechanical properties of the silk are needed to guarantee optimum activity.

Graphical abstract

Corresponding author: carole.perry@ntu.ac.uk, Tel: +0044 115 8486695 (no FAX available).

Keywords

silk; FTIR spectroscopy; Thioflavin T; conformational change; hydrogen bonding

1.1 Introduction

Silk is a biomolecule which has been utilised for possibly as long as a millennium in medical procedures [1] and still continues to be developed and modified for a myriad of potentially new applications [2–6]. Silk materials have high biocompatibility and versatility allowing a range of material forms to be fabricated; from fibres through to films, gels, sponges and non-woven mats with potential use in medical devices through to coatings for the preservation of perishable food products under ambient conditions [7,8]. Silk possesses high tensile strength and elasticity due to the naturally occurring beta sheet features of the proteins when formed into fibres or other forms [9]. The percentage of beta conformers, (sheet, aggregate and turn – a glossary of beta structure is included in the supplementary data p 1–2), are directly related to the physical properties exhibited by the silk, therefore it is important to be able to measure and customise the beta content of such materials.

In the analysis of protein conformation and conformational change a number of techniques are available (circular dichroism, X-ray analysis, nuclear magnetic resonance, infrared spectroscopy and thermal analysis) but generally each is subject to or requires control of the protein environment (solid or solution state). Reviewing the available literature on protein conformation analysis concludes that one of the most straightforward and widely available techniques is infrared spectroscopy. The use of Fourier self-deconvolution and peak fitting is an established method for analysing spectra with overlapping bands enabling the semi-quantitative estimation of the underlying components, but there is no fixed methodology for either process and they are subject to noise in their isolation of peak maxima and number [10–20]. Two dimensional infrared methods are also used in the quantitation of protein conformers with promising results but require more specialized equipment and operator experience.[21,22]

Much of the published data uses different fitting approaches and parameters for both spectral pre-treatment and the subsequent peak fitting and conformer identification often resulting in different conformational profiles and sometimes poorly and/ or erroneously fitted data. A significant contributory factor to this variability can be the manual imposition of peak parameters such as peak shape, position and width along with smoothing and deconvolution

methods or second derivative methods. Often the parameters are modified to give the best statistical fit with the experimental spectrum envelope with insufficient consideration of the validity of the individual peaks having a rational basis, and this can be a major obstacle especially for an inexperienced operator. Although some adjustment is always going to be necessary when comparing proteins in solid or solution phases due to changes in internal hydrogen bonding and water binding associated with the peptide backbone. It should still be possible to produce a single set of parameters which can be used to compare proteins undergoing conformational change in similar environments, such as annealing films and aqueous gelling processes. Indeed esteemed authors have questioned the level of autonomy of spectral fitting [17,18] and stated the desirability for processes with less operator influence and therefore greater objectivity. Furthermore, it would be advantageous for researchers in other disciplines to be able to extract meaningful data from spectra where the levels of expertise in spectroscopy and fitting processes may vary.

As silk can be reprocessed this means that it is different to many artificial polymers whose properties are fixed during fabrication *via* irreversible curing processes [23,24]. The fibres are highly ductile and comparable to the best synthetic materials such as nylon and polypropylene [25] but the latter are insoluble in water and hard to reprocess. Natural silk fibres, in contrast can be reprocessed after regenerating the fibroin. The regeneration process breaks up the β sheet structure of the spun fibroin by initial swelling and then disruption of the inter and intramolecular hydrogen bonding between the β strands and anti-parallel β sheets [26–29]. After regeneration, return to the favoured β structures can be prevented by processes such as rapid desalting using dialysis or desalting columns and immediate freeze-drying [30]. Provided the β sheet content is significantly reduced during reprocessing the fibroin remains soluble in a range of solvents including water, aqueous buffers, organic acids such as formic acid [31] and some organic solvents such as hexafluoroisopropanol and hexafluoroacetone [32]. From these solutions, fibroin can be reprocessed by spinning, gelling and dry casting methods [33] however the materials fabricated in this way will lack some of the tensile properties of the original silk due to reduction in the β sheet content. The process can largely be reversed by annealing which typically involves thermal or chemical treatment of the regenerated fibroin and generates intermolecular β sheet aggregates, which are largely responsible for the physical strength, elasticity and water insolubility of spun silk [34–37]. By monitoring the efficiency of annealing processes methods can be developed to fine-tune the material properties of silk materials. Extending their already wide range of uses; particularly in the biomedical field where ideal sample properties vary not only in the area of the body where the material is to be used, the device function but also from patient to patient. Controlling the conformational conversion from disordered/ helical to high β content enables the preparation of silks with contrasting physical and solution properties, which are required in these fields. As examples, implants such as support structures in bone repair and sustained drug release require different properties for optimum usage [38–42].

1.2 Infrared analysis: Origin of the amide I band and factors affecting frequency

Infrared absorption bands originate through various bond vibrational modes where there is a change in the dipole moment of the interacting groups within a molecule. These vibrational modes obey Hooke's law (i) and behave as harmonic oscillators:

$$\nu = \frac{1}{2\pi c}\sqrt{\frac{k}{\mu}} \quad (i)$$

ν = Frequency

c = Speed of light

k = Bond force constant

μ = Reduced mass = $\frac{m1 \cdot m2}{m1 + m2}$

Since m1 and m2 are the masses of the interacting oscillating bodies and k is the force constant, which is a measure of the bond strength, changes in these, will result in a frequency shift to the absorbance band. The amide I band originates largely from the peptide backbone carbonyl C=O stretching frequency with a small contribution from C-N stretch and C-C-N deformations. This is shifted significantly from the amino acid carbonyl frequency due to electron density changes brought about by carbanion resonance stabilisation [43]. The strength of the carbonyl bond can also be affected by the electronegativity of other adjacent molecules or elements (the inductive (I) effect) [44]. An increase in electron density brought about by the adjoining species (+I) will result in a weakening and lengthening of the carbonyl bond and hence a reduction in its frequency. Of the two effects, the resonance effect dominates and as the inductive effect operates over two carbon-carbon bonds, its effect is further diminished. What is significant, however, since conformational change results in no oscillator mass change or significant inductive effect in peptide bonds, is the effect of hydrogen bonding on the amide I bond strength and observed frequency. It was Pauling, Corey and Branson [45,46] who first recognised the role of hydrogen bonding in fixing protein conformations such as the helical and pleated sheet structures and noticed that these are subject to local media conditions. Dilute solutions and polar solvents tend to favour hydrogen bonding of the peptide carbonyl and N-H groups with water molecules. Where the amino acid residues are more hydrophobic it is entropically favourable to exclude water from the structure, form intra-molecular and, at higher concentration, inter-molecular hydrogen bonds. During drying processes, this can result increasingly in the formation of α helical and β sheet structures. Since conformational

change can be a relatively slow process, fast drying may fix some thermodynamically stable transitions in their higher energy state, thus rapid drying or drying under constrained conditions such as freeze drying can result in quasi-stable conformer mixes. These can be higher in random coil nature than they would achieve if allowed to attain a lower energy state if dried more slowly or without motional constraint. The competing processes result in a change in the C=O frequency which correlates with the length of the hydrogen bond [47]. Reduction in the amide I band frequency is caused by the C=O stretch band through hydrogen bonding strength changes and changes in bond angles of the C-N stretch, C-C-N deformations and N-H stretch [48]. In addition to the commonly reported β sheet and turn structure it is also possible to identify the β aggregate structure which enhances the amide I band envelope at around 1615 cm^{-1} and is largely the result of inter-molecularly hydrogen bonded β sheet. This is a large component of crystalline silk beta domains and as such provides much of the structural rationale for the high tensile strength and elasticity of silk fibroin [49]. It is these such structures common in protein fibrillation which provide the binding sites required for staining techniques using Thioflavin T or Congo red for example which are commonly used in the identification of amyloid plaques [50–52]. Thus, such a staining approach can be used to confirm time dependent conformational changes assessed by FTIR-ATR spectroscopy.

The aim of this investigation was to produce a simplified method for protein conformational analysis producing clear unequivocal results that are reproducible and require a minimum of user manipulation such that it would be suitable for scientists working in interdisciplinary fields where expertise may be limited. Peak fitting of the amide I band during the silk fibroin film annealing process was carried out to reproducibly determine changes in the protein conformation with time. An iterative process whereby the effect that one independent parameter change had on the fitting outcome was employed. Variables (peak position, width, shape, conformer abundances at start of iteration), were statistically compared with the result that an optimum set of parameter choices for protein conformational analysis could be defined. These parameters were applied initially to a freshly cast silk film to compare effects of the individual parameter changes to the fitting and reproducibility and the optimised parameters then applied to a set of proteins of contrasting secondary structure properties before finally applying them to spectra collected during the silk annealing process. The use of a range of reference proteins shows the approach to be applicable not just to the conformer variation we would expect to see during silk annealing but also to unrelated solid state proteins, and this was achieved without manual adjustment of the fitting parameters.

2. Materials and Methods

2.1 Materials

Materials were obtained as follows. Protein reference materials γ globulin, bovine serum albumin (BSA), α lactalbumin, sodium bicarbonate (NaHCO$_3$ 99%+), lithium bromide (LiBr 99%+), cellulose dialysis tubing (MWCO 12–14kDa), and Thioflavin T 65–75% dye, from Sigma-Aldrich, (Dorset, UK). *Bombyx mori* dewormed silk cocoons from Forest Fibres, (Gloucester, UK). Deionised water (< 10 μScm^{-1}) single distilled and deionised with

a single pass ion exchange resin, (Elga micromax, High Wycombe UK). Sodium hydroxide (NaOH 97%+) and methanol (99%+) from Fisher Scientific, (Loughborough, UK).

2.2 Methods

2.2.1 Reference protein preparation—The reference proteins were sampled as received (dry free flowing white powders) and cast on clean dry microscope slides from a single 10 μL drop of a 10% aqueous protein solution. A minimum of 5 independent samples were prepared for all proteins.

2.2.2 Silk film preparation—Dewormed *Bombyx mori* cocoons (2% w/v) were degummed in 0.5% w/v sodium bicarbonate solution by boiling for 30 minutes, draining and repeating before thoroughly rinsing with deionised water and drying at room temperature. The silk fibroin (20% w/v) was then solubilised in lithium bromide solution (9.3 M) at 60 °C for 3 hours. After cooling the silk solution was dialysed against sodium hydroxide solution (10^{-4} M, pH 10) (1:100 solution to dialysate) with an additional 4 changes of dialysate over 8 hours to give a final silk concentration of 10% w/v. The silk solution prepared in this way remained stable against gelation for at least 1 week at 4 °C. Films were prepared by adjusting the pH of a small aliquot of the silk solution to 7.0 with hydrochloric acid and spotting 10 μL of the solution on to a clean dry microscope slide and drying under normal air flow overnight forming an approximately 5 mm disk with a raised annulus. Annealing of the silk films was carried out in a reduced pressure methanol water atmosphere (60% methanol$_{(v/v)}$ in open petridishes (4×9 cm diameter) each containing 20 mL of the aqueous methanol, in a 35 L vacuum oven at 635 mBar and 25 °C) for times ranging from 5 minutes to 24 hours. The annealed films were then left to equilibrate in air at 25 °C for 24 hours before any spectroscopy or staining was attempted.

2.2.3 Fourier transform infrared attenuated total reflectance spectroscopy (FTIR-ATR)—Spectra were collected using a Perkin Elmer spectrum 100 spectrophotometer (Perkin Elmer spectrum 2012, v.10.03.07 software) with a single reflection diamond crystal universal ATR sampling accessory. Five replicate powders or films (specifically the annulus) were individually measured and fitted for statistical analysis. Figure 1 shows 5 overlaid replicate spectra of non-annealed silk fibroin films and Figures 1b/c represent the peak fitting and reproducibility of the fitting respectively. All spectra were collected between 4000 and 500 cm^{-1} at a resolution of 4 cm^{-1} accumulated from 16 individual scans. They were zero baseline adjusted at multiple points including a single linear section between 1730 cm^{-1} and 1470 cm^{-1} to cover the amide I and amide II region of interest.

Curve fitting was performed using Thermo grams A1 software V.8. The final chosen parameters included peaks and fixed absorbance wavelength maxima selected [14, 35–37] at 1712 cm^{-1} (side chains), 1693 cm^{-1} (intermolecular β sheet), 1680 cm^{-1} (β turn), 1656 cm^{-1} (random coil), 1644 cm^{-1} (α helix) 1628 cm^{-1} (intramolecular β sheet) 1615 cm^{-1} (intermolecular β sheet) and 1592 cm^{-1} (a peak introduced to compensate for non-baseline resolution of the amide I and II bands without discrimination against lower frequency components). All peaks were half height width limited to between 10 and 30 cm^{-1} but

allowed to assume any positive height/area. The conformer composition was calculated as the area of the relevant peak as a percentage of the total amide I peak area. For comparison, the same spectra presented in Figure 1 were also treated using a deconvolution approach; details on the method adopted and the results can be found in the Supplementary Information and Figure S1.

We have used the notation of C=O as an abbreviation of the amide I band but the calculated energy change is as a direct consequence of the change in the population of the conformer bands coupled with their frequencies which are a composite of the various vibrational modes. The resulting energy change (calculation methodology detailed in the SI) observed with annealing time we feel then gives a simple single point measure of the progression of the annealing process.

2.2.4 Statistical analysis—Unless otherwise stated five independent samples were prepared, measured and the resulting spectra fitted. During model development, the influence of variable parameters on the goodness of fit with the experimental spectrum were assessed based on the reduced chi square (x_ν^2) using the Thermo grams A1 software V.8. and standard deviation statistics generated using Microsoft office excel 2013.

2.2.5 Thioflavin T amyloid staining—Thioflavin T (8 mg) was dissolved in pH 7 phosphate buffer (1 M), filtered through a 0.2 μm membrane and diluted to 1 in 50 to generate the working solution. Aliquots of 10% silk solution (10 μL) were applied to give complete coverage of glass microscope slide covers (6 mm diameter) and allowed to dry at room temperature overnight before annealing for up to 24 hours as described above. Staining was performed by immersing the films in 200 μL of working Thioflavin T solution for 10 minutes and then washing with 3×200 μL of deionised water before air drying as before. Comparisons of staining intensity were made visually and under UV irradiation at 360 nm excitation [53], monitoring the emission spectrum from 400 – 800 nm.

3. Results and Discussion

3.1 Method development using *B. mori* silk fibroin

Replicate silk fibroin films were prepared as described in the methods section and the resulting spectra normalised and plotted on a single graph (Figure 1a) to demonstrate their similarities.

Spectral parameters were chosen according to literature precedence [17, 54–56] and the final selected conditions listed in the materials and methods. Thioflavin T staining was used to provide evidence for the rationale of the specific inclusion of the β aggregate (1615 cm^{-1}) absorbance peak.

The suitability of chosen parameters was determined by measurement of both goodness of fit (reduced chi square (x_ν^2) regression analysis), Figure 1b and agreement of results from 5 replicate spectra presented as square root mean variance of the individual conformer peaks fitted, Figure 1c. When using x_ν^2 analysis, lower values are indicative of improved agreement

of the model with the experimental spectrum however, values < 1 generally indicate noise fitting. Typically, peak fitting analysis includes the use of Fourier self-deconvolution for resolution enhancement [57]. However, consequences of this treatment can include side lobe formation due to over deconvolution and noise increase [58]. Noise is particularly problematic as small perturbations due to background water vapour are rapidly magnified by the processing. The resulting peak picking tends then to be subject to the choice of processing step size in peak position and width. Applying narrow step changes between iterations results in peak pinning but using wider step changes can result in unreasonable spectral drift both of which result in erroneous fitting and incorrect wavelength maxima positions. Peak fitting was therefore conducted without deconvolution, smoothing or automatic peak picking by instead imposing confined peak positions and widths for the underlying conformational sources of the amide I envelope.

The variables (peak position, width, shape, conformer abundances at start of iteration) were assessed independently for their effect on the resulting statistical analyses.

3.1.1 Peak Shape—Gaussian, Lorentzian and mixed Gaussian/ Lorentzian (Voigt) [18] peak shapes were compared. Gaussian peak shape showed better fit with the experimental spectra than Lorentzian peak shape based on values of reduced chi square, Figure 1b. Mixed Gaussian/Lorentzian peak character was also investigated and gave better reduced chi square results, Figure 1b, however on inspection, the peaks were largely Gaussian in nature and also showed greater sample to sample variation compared to pure Gaussian fitting alone, Figure 1c, given this, a pure Gaussian fit was selected.

3.1.2 Pre-biased conformer fitting—The initial state for the fitting process was found to affect the outcome/convergence of the fit where either an initial bias was placed on one conformer over the other or no bias was applied. Here we applied a bias on the β structure related peaks or on the α helical/random coil, related peaks or both were set at the same initial level. Figure 1b shows that regardless of whether bias was imposed or not there was little impact on the regression results and when the replicate spectra were compared, Figure 1c again there was little difference provided the conformer wavelength maxima positions were fixed. Interestingly when a random/ helical bias was imposed, the selection of peak shape made no difference to the outcome of the variance.

3.1.3 Fixed Peak Position and Peak Area—Allowing a fixed level of freedom of movement for the various protein conformer wavenumber maxima positions produced an improved reduced chi square (χ^2_ν) for the fitting process but also caused an increase in variance overall which was a result of peak 'pinning' at local minima caused by the presence of spectral noise, Figure 1b/c. For this reason, the conformers were prevented from drifting to these minima by confinement to the centre of their literature ranges [17, 54–56] and then allowed freedom to expand to any height/area. Limiting the half height width to between 10 and 30 cm^{-1} also enabled both acceptable reduced chi square fitting of the spectral envelope and also good replication of conformer make up of silk spectra, Figure 1b and c. Not limiting the peak widths either resulted in noise fitting in the absence of a minimum limit or

peaks of unreasonably large width spanning the amide I and II regions in the absence of an upper limit. The experimental design and outcomes are shown in Figure 2.

Optimum parameters for the best fitting of the experimental peaks and lowest standard deviation of the 5 replicate sample spectra were thus determined. The final conditions selected were chosen for their ability to clearly distinguish between similar but not identical spectra, Figure 1a and consistently do this for multiple replicate samples.

3.2 Validation of approach for proteins with contrasting secondary structure compositions

Reference proteins were selected based on their varying levels of β sheet structure in their native forms. γ Globulins are known to contain relatively high levels of β sheet structure whilst BSA has very little primary structure of a β nature [59] and the conformation of α lactalbumin lies somewhere between the two. However, in their solid state these proteins are unlikely to exhibit true native secondary structure so they were measured both as, as received powders and as films dried passively from water overnight to allow conformational change to occur. The peak fitting methodology was aimed specifically to contrast the different conformational compositions of the proteins and to be able to monitor process-induced change in conformation.

When applied to the selected reference proteins the example fitting for α lactalbumin, Figure 3, gives excellent fits (reduced chi square, χ_ν^2) with the experimentally derived spectra, Figure 4. Statistical comparisons based on one-sigma confidence limits also shows clearly significant differences between the replicate data sets of both the BSA and α lactalbumin compared with the γ globulin in terms of the conformational composition, as powders and as films. This also shows differences between BSA and α lactalbumin, but differences between pre and post drying were less significant, Figure 4. The conformation data for BSA based on X-ray crystallography of homologous proteins (equine and human serum albumins) [60] shows it to be highly helical in structure (~75%) and circular dichroism of fragments indicate no more than 20% beta structure [61] but here we find higher levels of the latter. These values are highly dependent upon physical state and environmental effects (dry, hydrated or solvent/dispersant) so sample preparation will have a significant effect on the conformational outcome. Other studies have shown that BSA even in the absence of formal primary β structure does give infrared spectra consistent with significant (~30%) β aggregate nature under denaturing conditions of elevated temperatures, increased ionic strength and drying [62,63], in general agreement with our findings. By contrast, the β sheet content found here for γ globulin is lower than reported from X-ray analysis and circular dichroism [64,65]. Which may be due to our drying process being too rapid for thermodynamic relaxation of the structure but may also be a function of the propensity of globular proteins to form intra-molecular β sheet structure in preference to extended inter-molecular β aggregates [66]. The sum of the β characteristic bands found (~57%) by peak fitting is in agreement with published data (Supplemental data Table 1) although it is clear that conformer values determined by each of the methods are highly dependent on pre-treatment for all the proteins. BSA and γ globulin both showed the same trend of more β aggregate spectral content after film preparation suggesting that they exhibit, to some extent this slow thermodynamic change during drying, behaviour which can also be expected for regenerated

silk fibroins. α lactalbumin by contrast showed much less clearly defined change, and these observations may be indicative of the extraction and recovery processes used in the commercial production of the proteins.

The outcome of the peak fitting process and differences observed between the proteins were in agreement with what may have been expected purely by visual inspection and observer expectation of the spectra but no operator input was made thus maintaining the objectivity of the process.

3.3 Spectroscopy of the silk annealing process

The glycine (G) and alanine (A) content of *Bombyx* fibroin constitute approximately 75% per mole, the vast majority of which are linked through 11 highly conserved charged domains of 30–31 amino acid residues, which include the sequence GPYVA/N. The presence of proline (P) provides for a more flexible β turn with potential for the silk to form an anti-parallel β sheet structure, and we have therefore included the turn conformer in our estimation of total β content. Thus, there is a propensity for a large amount of β structure in fully annealed regenerated silk fibroin films with studies by solid-state ^{13}C CP-MAS NMR spectroscopy showing in excess of 75% of the alanine present to be in a β arrangement [67]. By extrapolation if we include closely associated glycine residues, we should expect 60% or more of the fibroin to be represented by β conformers. The *Bombyx mori* amino acid sequence also contains 7% of residues with side chain functionality that could interfere in the amide I region but only 1% of the total residues are strong (acidic carbonyl) absorbers. The contribution of any such acidic residues should be removed from the amide I band conformational content by subtraction of the 1712 cm^{-1} band during peak fitting. The amide I region observed for the silk fibroin should therefore be largely independent of such side chain interference after treatment.

Alcoholic treatment of regenerated silk fibroin is known to promote the formation of β structure [68,69] and spectral changes were observed during the annealing process employed in this study, (Supplemental data Figure S2) indicating the expected transition from random and helical structure to a more β dominated structure, Figures 5a,b. The fitting process presented herein allowed us to monitor the conformational changes without any change to the initial fitting parameters thereby generating results free of operator subjectivity.

Increased levels of intermolecular β sheet structure was observed within the first ten minutes of the start of the annealing process which was also accompanied by an initial increase of the less strongly hydrogen bonded conformers (random coil and helical structures) probably as a consequence of the swelling of the dried fibroin on penetration by methanolic water vapour [70]. Over the next 60 minutes or so, β sheet and β aggregate levels increased as reduction in all the less strongly hydrogen bonded structures continued probably by a progressive change from random coil to a helical structure and/or intramolecular β sheet and ultimately intermolecular β sheet. The level of crystallinity/aggregate found overall (as the sum of the β structures) was in agreement with other published work using infrared spectroscopy or other methods for quantitation, Table 1. Although structural changes were observed to continue for up to 24 hours, the vast majority of the restructuring took place in the first 2 hours of the treatment. In addition, over this time the proportion of β turn to

aggregate decreased indicative of the formation of larger crystalline domains as a result of intermolecular hydrogen bonding which has been described previously both *in vivo* and *in vitro* during silk spinning processes [71,72].

Confirmation of the presence of β aggregate domains was also shown by Thioflavin T staining, Figure 6 with the development of a visible yellow colour and emission signal at 485 nm indicative of the formation of amyloid/ β aggregate structure.

The staining observed was the result of two processes, 1) the absorption and re-orientation of the Thioflavin T dye on the β aggregate crystallites resulting in the characteristic emission shift and enhancement observed and, 2) the decreased solubility of the annealed silk films as a result of their increased β structure. At the shorter annealing times (before ca. 10 minutes) the films were water soluble and were removed from the glass coverslips during the staining and washing process, so staining was not observed though infrared analysis suggests presence of β aggregates, Figures 5a, b and 6. After 30 minutes or more the films became increasingly insoluble and staining indicative of β aggregates was readily observed by fluorescence measurement or the naked eye, Figure 6. Fitting of simple exponential functions to the curves (supplementary data figure S7) showed a rather poor fit initially and a closer fit at longer annealing times. This suggests that there are two processes operating in both of the methods used to determine conformational change. Both methods show a lag or delay at the onset of the annealing process. The energy change error from the data is indicative of the swelling of the silk matrix prior to re-organisation of the β structure. This corresponds with the reported behaviour of fibres treated with solvent vapour [70] and the variation in Thioflavin T staining is a function of both this and the solubility of the fibroin with shorter annealing times. Suggesting that the fibroin was still at least partially soluble up to 60 minutes after the start of annealing.

3.4 Conversion of spectroscopic output to energy change

In addition to the conformational analysis in terms of relative percentages of the conformers, we were also able to measure the amide I bond energy changes resulting from changes in the strength of hydrogen bonding as the silk conformational assemblage changed. The structural changes observed arise from a change in the amide carbonyl vibrational energy due to changes in the hydrogen bonding pattern associated with development of the β structure. We used this frequency change to calculate the energy change associated with the annealing process. As a reference, we considered using the random coil condition as the reference frequency (1656cm^{-1}) since this consists of only intramolecular hydrogen bonding and does not significantly add to the overall bulk structural stabilisation of the silk materials. Alternatively we compared reference values obtained for non-hydrogen bonded proteins in dimethylsulphoxide (DMSO) solutions, which have been observed to occur at 1662 cm^{-1} at high dilution [76]. For this study, we chose the latter and therefore the data presented includes a small contribution from the random coil energy change involved in the stabilisation of the fibroin structure. However, the close proximity of it to the non-hydrogen bonded state means its influence on the calculated energy changes is small and it is the intermolecular β sheet hydrogen bonding contribution which dominates.

Calculation of the change in hydrogen bonding energy (detailed in the SI) for the silk films at various stages of annealing enabled the progression of the process to be observed very clearly, Figure 5d and showed a clearer correlation with the β aggregate staining more clearly than when observing changes of the individual conformers, Figure 5c.

During annealing, the bond frequency energy change results in a decrease of ~80 Jmol^{-1} on average per backbone carbonyl which equates to ~400 KJmol^{-1} of fibroin and represents a large contribution to the structural stabilisation of the macroscopic structure, Figure 5d. As the hydrogen bonds providing this stabilisation are individually comparatively weak the large reservoir of total energy transfer means that, the silk has a large capacity to un-zip along the β crystallites when extended without breaking the primary protein structure. However, to produce the tensile and elastic properties observed for the naturally spun fibre [77] the crystallites need to be aligned along the axis of extension.

4. Conclusions

Peak fitting of spectra for silk fibroin and three 'model' proteins was achieved without the use of peak deconvolution and optimised parameters reported. The conformational make up of each 'model' protein was compatible with many published results for these proteins held under various conditions [60–66] particularly where β structure is favoured (i.e. when dried or thermally denatured).

For silk fibroin, the changes induced by the annealing process produced measurable effects at all stages of the process. Initially changes appeared to correlate with those expected during swelling of the silk fibroin and although a modest increase of random and helical nature was observed, it was still associated with an overall transfer of energy to hydrogen-bonded structures commensurate with an increase in β content. Understanding the nature of the changes in hydrogen bonding patterns enabled us to make use of the energy change calculated from the amide I carbonyl shift to follow the progress of the annealing process more clearly than by monitoring one or all of the changing conformers. This indicated that annealing results in a progressive weakening of the carbonyl band, over the course of ca. 24 hours. The majority of the change was through the formation of β aggregate structures in the first 2 – 3 hours of annealing but further small but significant changes were observed for up to 24 hours. We were able to estimate the hydrogen bond stabilization of the fibroin to be ~400 KJmol^{-1}, analogous to the energy required to heat 1 kg of water from 0 °C to boiling point (at 1 atm). This energy can be released mechanically by unzipping of the aligned β aggregate crystallites and explains the tensile properties of silk [25]. We suggest that the peak fitting method outlined in this contribution can be used as an experimental aid in the development of silk based materials for biomedical applications where tuning of the physical and mechanical properties of the silk are needed to guarantee optimum activity.

Supplementary Material

Refer to Web version on PubMed Central for supplementary material.

Acknowledgments

References

1. Mackenzie D. The history of sutures. Medical History. 1973; 17(2):158–168. [PubMed: 4578411]

2. Hakimi O, Knight DP, Vollrath F, Vadgama P. Spider and mulberry silkworm silks as compatible biomaterials. Composites Part B: Engineering. 2007; 38(3):324–337.

3. Altman GH, Diaz F, Jakuba C, Calabro T, Horan RL, Chen J, Lu H, Richmond J, Kaplan DL. Silk-based biomaterials. Biomaterials. 2003; 24(3):401–416. [PubMed: 12423595]

4. Borkner CB, Elsner MB, Scheibel T. Coatings and films made of silk proteins. ACS Applied Materials and Interfaces. 2014; 6(18):15611–15625. [PubMed: 25004395]

5. Shimanovich U, Ruggeri FS, De Genst E, Adamcik J, Barros TP, Porter D, Müller T, Mezzenga R, Dobson CM, Vollrath F, Holland C, Knowles TPJ. Silk micrococoons for protein stabilisation and molecular encapsulation. Nature Communications. 2017; 8(15902):1–9.

6. Smitthipong W, Suethao S, Shah D, Vollrath F. Interesting green elastomeric composites: Silk textile reinforced natural rubber. Polymer Testing. 2016; 55:17–24.

7. Vepari C, Kaplan DL. Silk as a biomaterial. Progress in Polymer Science. 2007; 32(8):991–1007. [PubMed: 19543442]

8. Marelli B, Brenckle MA, Kaplan DL, Omenetto FG. Silk Fibroin as Edible Coating for Perishable Food Preservation. Nature Scientific Reports. 2016; 6:25263, 1–11.

9. Gosline JM, Guerette PA, Ortlepp CS, Savage KN. The mechanical design of spider silks: from fibroin sequence to mechanical function. The Journal of Experimental Biology. 1999; 202(23): 3295–3303. [PubMed: 10562512]

10. Cerf E, Sarroukh R, Tamamizu-Kato S, Breydo L, Derclaye S, Dufrêne YF, Narayanaswami V, Goormaghtigh E, Ruysschaert J-M, Raussens V. Antiparallel β-sheet: a signature structure of the oligomeric amyloid β-peptide. Biochemical Journal. 2009; 421(3):415–423. [PubMed: 19435461]

11. Broersen K, Jonckheere W, Rozenski J, Vandersteen A, Pauwels K, Pastore A, Rousseau F, Schymkowitz J. A standardized and biocompatible preparation of aggregate-free amyloid beta peptide for biophysical and biological studies of Alzheimers disease. Protein Engineering, Design and Selection. 2011; 24(9):743–750.

12. Kamalha E, Zheng Y, Zeng Y. Analysis of the secondary crystalline structure of regenerated Bombyx mori fibroin. Research & reviews in Biosciences. 2013; 7(2):76–83.

13. Litvinov RI, Faizullin DA, Zuev YF, Weisel JW. The α-helix to β-sheet transition in stretched and compressed hydrated fibrin clots. Biophysical Journal. 2012; 103(5):1020–1027. [PubMed: 23009851]

14. Barth A. Infrared spectroscopy of proteins. Biochimica et Biophysica Acta - Bioenergetics. 2007; 1767(9):1073–1101.

15. Matsumoto A, Chen J, Collette AL, Kim UJ, Altman GH, Cebe P, Kaplan DL. Mechanisms of silk fibroin sol-gel transitions. Journal of Physical Chemistry B. 2006; 110(43):21630–21638.

16. Speare JO, Rush TS. IR spectra of cytochrome c denatured with deuterated guanidine hydrochloride show increase in β sheet. Biopolymers. 2003; 72(3):193–204. [PubMed: 12722115]

17. Goormaghtigh E, Cabiaux V, Ruysschaert JM. Secondary structure and dosage of soluble and membrane-proteins by attenuated total reflection fourier-transform infrared-spectroscopy on hydrated films. European Journal of Biochemistry. 1990; 193:409–420. [PubMed: 2226461]

18. Hering, JA., Haris, PI. FTIR spectroscopy for analysis of protein secondary structure. In: Barth, A., Haris, PI., editors. Biological and Biomedical Infrared Spectroscopy. IOS press; Amsterdam: 2009. p. 129-167.

19. Li C, Kumar S, Montigny C, le Maire M, Barth A. Quality assessment of recombinant proteins by infrared spectroscopy. Characterisation of a protein aggregation related band of the Ca^{2+}-ATPase. The Analyst. 2014; 139(17):4231–40. [PubMed: 24965041]

20. Byler DM, Susi H. Examination of the secondary structure of proteins by deconvolved FTIR spectra. Biopolymers. 1986; 25(3):469–487. [PubMed: 3697478]

21. Baiz CR, Peng CS, Reppert ME, Jones KC, Tokmakoff A. Coherent two-dimensional infrared spectroscopy: Quantitative analysis of protein secondary structure in solution. The Analyst. 2012; 137(8):1793–1799. [PubMed: 22398665]

22. Ganim Z, Chung HS, Smith aW, Deflores LP, Jones KC, Tokmakoff A. Amide I Two-Dimensional Infrared Spectroscopy of Proteins. Accounts of chemical research. 2008; 39(25):432–441.

23. Decker C. Photoinitiated crosslinking polymerisation. Progress in Polymer Science. 1996; 21(4): 593–650.

24. Oyama, T. Cross-Linked Polymer Synthesis. In: Kobayashi, S., Müllen, K., editors. Encyclopedia of Polymeric Nanomaterials. Heidelberg: Springer Berlin Heidelberg; 2014. p. 1-11.

25. Koh L, Cheng Y, Teng C, Khin Y, Loh X, Tee S, Low M, Ye E, Yu H, Zhang Y, Han M. Progress in Polymer Science Structures, mechanical properties and applications of silk fibroin materials. Progress in Polymer Science. 2015; 46:86–110.

26. Phillips DM, Drummy LF, Conrady DG, Fox DM, Naik RR, Stone MO, Trulove PC, De Long HC, Mantz RA. Dissolution and regeneration of Bombyx mori silk fibroin using ionic liquids. Journal of the American Chemical Society. 2004; 126(44):14350–14351. [PubMed: 15521743]

27. Cebe P, Hu X, Kaplan DL, Zhuravlev E, Wurm A, Arbeiter D, Schick C. Beating the heat-fast scanning melts silk beta sheet crystals. Scientific Reports. 2013; 3:1–7.

28. Boulet-Audet M, Holland C, Gheysens T, Vollrath F. Dry-Spun Silk Produces Native-Like Fibroin Solutions. Biomacromolecules. 2016; 17(10):3198–3204. [PubMed: 27526078]

29. Wang H-Y, Zhang Y-Q. Effect of regeneration of liquid silk fibroin on its structure and characterization. Soft Matter. 2013; 9(1):138–145.

30. Ha SW, Tonelli AE, Hudson SM. Structural Studies of Bombyx mori Silk Fibroin during Regeneration from Solutions and Wet Fibre Spinning. Biomacromolecules. 2005; 6(3):1722–1731. [PubMed: 15877399]

31. Zafar MS, Belton DJ, Hanby B, Kaplan DL, Perry CC. Functional Material Features of Bombyx mori Silk Light vs. Heavy Chain Proteins. Biomacromolecules. 2015; 16(2):606–614. [PubMed: 25565556]

32. Ha SW, Asakura T, Kishore R. Distinctive Influence of Two Hexafluoro Solvents on the Structural Stabilization of Bombyx mori Silk Fibroin Protein and Its Derived Peptides: 13C NMR and CD Studies. Biomacromolecules. 2006; 7(1):18–23. [PubMed: 16398492]

33. Rockwood DN, Preda RC, Yücel T, Wang X, Lovett ML, Kaplan DL. Materials fabrication from Bombyx mori silk fibroin. Nature Protocols. 2011; 6(10):1612–1631. [PubMed: 21959241]

34. Hu X, Shmelev K, Sun L, Gil ES, Park SH, Cebe P, Kaplan DL. Regulation of Silk Material Structure by Temperature-Controlled Water Vapor Annealing. Biomacromolecules. 2011; 12(5): 1686–1696. [PubMed: 21425769]

35. Karve KA, Gil ES, McCarthy SP, Kaplan DL. Effect of β-sheet crystalline content on mass transfer in silk films. Thin Films. 2012; 383:44–49.

36. Tsukada M, Gotoh Y, Nagura M, Minoura N, Kasai N, Freddi G. Structural changes of silk fibroin membranes induced by immersion in methanol aqueous solutions. Journal of Polymer Science Part B: Polymer Physics. 1994; 32(5):961–968.

37. Chen X, Cai H, Ling S, Shao Z, Huang Y. Conformation transition of bombyx mori silk protein monitored by time-dependent fourier transform infrared (FT-IR) spectroscopy: Effect of organic solvent. Applied Spectroscopy. 2012; 66(6):696–699. [PubMed: 22732542]

38. Meinel L, Fajardo R, Hofmann S, Langer R, Chen J, Snyder B, Vunjak-Novakovic G, Kaplan DL. Silk implants for the healing of critical size bone defects. Bone. 2005; 37(5):688–698. [PubMed: 16140599]

39. Wang Y, Kima H, Vunjak-Novakovicb G, Kaplan DL. Stem cell-based tissue engineering with silk biomaterials. Biomaterials. 2006; 27(36):6064–6082. [PubMed: 16890988]

40. Lawrence, BD. Processing of Bombyx mori silk for biomedical applications. In: Kundu, SC., editor. Silk Biomaterials for Tissue Engineering and Regenerative Medicine. Woodhead Publishing; 2014. p. 78-99.

41. Numata, K. Silk hydrogels for tissue engineering and dual-drug delivery. In: Kundu, SC., editor. Silk Biomaterials for Tissue Engineering and Regenerative Medicine'. Woodhead Publishing; 2014. p. 503-518.(2014)

42. Mandal BB, Grinberg A, Seok Gil E, Panilaitis B, Kaplan DL. High-strength silk protein scaffolds for bone repair- Proceedings of the National Academy of Sciences. 2012; 109(20):7699–7704.

43. Pauling L. The Shared-Electron Chemical Bond. Proceedings of the National Academy of Sciences. 1928; 14(4):359–362.

44. Stock LM. The origin of the inductive effect. Journal of Chemical Education. 1972; 49(6):400–4.

45. Pauling L, Corey RB, Branson HR. The structure of proteins: Two hydrogen-bonded helical configurations of the polypeptide chain. Proceedings of the National Academy of Sciences. 1951; 37(4):205–211.

46. Pauling L, Corey RB. The Pleated Sheet, A New Layer Configuration of Polypeptide Chains. Proceedings of the National Academy of Sciences. 1951; 37(5):251–256.

47. Myshakina NS, Ahmed Z, Asher SA. Dependence of Amide Vibrations on Hydrogen Bonding. J Phys Chem B. 2009; 112(38):11873–11877.

48. Barth A, Zscherp C. What vibrations tell about proteins. Quarterly Reviews of Biophysics. 2002; 35(4):369–430. [PubMed: 12621861]

49. Cheng Y, Leng-Duei K, Dechang L, Baohua J, Ming-Yong H, Yong-Wei Z. On the Strength of β-Sheet Crystallites of Bombyx Mori Silk Fibroin. Journal of the Royal Society Interface. 2014; 11(96)

50. Puchtler H, Sweat F, Levine M. On the binding of Congo Red by Amyloid. Journal of Histochemistry & Cytochemistry. 1962; 10(3):355–364.

51. Hinds IL. Oxalic Acid-Crystal Violet Staining Method for Demonstration of Amyloid. Laboratory medicine. 1983; 14(5):5–7.

52. Biancalana M, Koide S. Molecular mechanism of Thioflavin-T binding to amyloid fibrils. Biochimica et Biophysica Acta (BBA) - Proteins and Proteomics. 2010; 1804(7):1405–1412. [PubMed: 20399286]

53. Freire S, De Araujo MH, Al-Soufi W, Novo M. Photophysical study of Thioflavin T as fluorescence marker of amyloid fibrils. Dyes and Pigments. 2014; 110:97–105.

54. Byler DM, Susi H. Examination of the secondary structure of proteins by deconvolved FTIR spectra. Biopolymers. 1986; 25(3):469–487. [PubMed: 3697478]

55. Kong J, Yu S. Fourier Transform Infrared Spectroscopic Analysis of Protein Secondary Structures Protein FTIR Data Analysis and Band Assignment. Acta Biochimica et Biophysica Sinica. 2007; 39(8):549–559. [PubMed: 17687489]

56. Chittur KK. FTIR/ATR for protein adsorption to biomaterial surfaces. Biomaterials. 1998; 19(4): 357–369. [PubMed: 9677150]

57. Yang WJ, Griffiths PR, Byler DM, Susi H. Protein Conformation By Infrared Spectroscopy: Resolution Enhancement By Fourier Self-Deconvolution. Applied Spectroscopy. 1985; 39(2):282–287.

58. Kauppinen, J., Partanen, J. Fourier Transforms in Spectroscopy. Wiley-VCH Verlag GmbH; 2001. p. 196-202.

59. Giacomelli CE, Bremer MGEG, Norde W. ATR-FTIR Study of IgG Adsorbed on Different Silica Surfaces. Journal of Colloid and Interface Science. 1999; 220(1):13–23. [PubMed: 10550236]

60. Majorek KA, Porebski PJ, Dayal A, Zimmerman MD, Jablonska K, Stewart AJ, Chruszcz M, Minor W. Structural and immunologic characterization of bovine, horse, and rabbit serum albumins. Molecular Immunology. 2012; 52(3–4):174–182. [PubMed: 22677715]

61. Reed, RG., Feldhoff, RC., Clute, OL., Peters, T. Biochemistry. Vol. 14. American Chemical Society; 1975. Fragments of bovine serum albumin produced by limited proteolysis. Conformation and ligand binding; p. 4578-4583.

62. Holm NK, Jespersen SK, Thomassen LV, Wolff TY, Sehgal P, Thomsen LA, Otzen DE. Aggregation and fibrillation of bovine serum albumin. Biochimica et Biophysica Acta. 2007; 1774:1128–1138. [PubMed: 17689306]

Author Manuscript

63. Murayama K, Tomida M. Heat-induced secondary structure and conformation change of bovine serum albumin investigated by fourier transform infrared spectroscopy. Biochemistry. 2004; 43(36):11526–11532. [PubMed: 15350138]

64. Gorinstein S, Zemser M, Friedman M, Chang SH-M. Simultaneous differential scanning calorimetry, X-ray diffraction and FTIR spectrometry in studies of ovalbumin denaturation. International Journal of Peptide and Protein Research. 1995; 45:248–256. [PubMed: 7775017]

65. Nag M, Das D, Bandyopadhyay D, Basak S. Unusual denaturation trajectory of bovine gamma globulin studied by fluorescence correlation spectroscopy. Physical Chemistry Chemical Physics. 2015; 17(29):19139–19148. [PubMed: 26136209]

66. Choi S, Ma C. Conformational Study of Globulin from Common Buckwheat (*Fagopyrum Esculentum Moench*) by Fourier Transform Infrared Spectroscopy and Differential Scanning Calorimetry. Journal of Agricultural and Food Chemistry. 2005; 53(20):8046–53. [PubMed: 16190669]

67. Ruan QX, Zhou P. Sodium ion effect on silk fibroin conformation characterized by solid-state NMR and generalized 2D NMR-NMR correlation. Journal of Molecular Structure. 2008; 883–884:85–90.

68. Chen X, Shao Z, Marinkovic NS, Miller LM, Zhou P, Chance MR. Conformation transition kinetics of regenerated Bombyx mori silk fibroin membrane monitored by time-resolved FTIR spectroscopy. Biophysical Chemistry. 2001; 89(1):25–34. [PubMed: 11246743]

69. Lawrence BD, Wharram S, Kluge JA, Leisk GG, Omenetto FG, Rosenblatt MI, Kaplan DL. Effect of hydration on silk film material properties. Macromolecular Bioscience. 2010; 10(4):393–403. [PubMed: 20112237]

70. Jeong L, Lee KY, Liu JW, Park WH. Time-resolved structural investigation of regenerated silk fibroin nanofibers treated with solvent vapor. International Journal of Biological Macromolecules. 2006; 38(2):140–144. [PubMed: 16545448]

71. Shen Y, Johnson MA, Martin DC. Microstructural characterization of Bombyx mori silk fibers. Macromolecules. 1998; 31(25):8857–8864.

72. Takahashi Y, Gehoh M, Yuzuriha K. Structure refinement and diffuse streak scattering of silk (Bombyx mori). International Journal of Biological Macromolecules. 1999; 24(2–3):127–138. [PubMed: 10342756]

73. Lerber KC, Von K, Wess T. Measuring crystallinity of laser-cleaned silk by X-ray diffraction. E-Preservation Science. 2005:31–37.

74. Kim SH, Nam YS, Lee TS, Park WH. Silk Fibroin Nanofiber. Electrospinning, Properties, and Structure. Polymer Journal. 2003; 35(2):185–190.

75. Boulet-Audet M, Lefèvre T, Buffeteau T, Pézolet M. Attenuated total reflection infrared spectroscopy: An efficient technique to quantitatively determine the orientation and conformation of proteins in single silk fibres. Applied Spectroscopy. 2008; 62(9):956–962. [PubMed: 18801233]

76. Jackson M, Mantsch HH. Beware of proteins in DMSO. Biochimica et Biophysica Acta (BBA) - Protein Structure and Molecular Enzymology. 1991; 1078(2):231–235. [PubMed: 2065090]

77. Du N, Liu XY, Nanan J, Li L, Lim LML, Li D. Design of Superior Spider Silk: From Nanostructure to Mechanical Properties. Biophysical Journal. 2006; 91(12):4528–4535. [PubMed: 16950851]

Statement of Significance

The physical and mechanical properties of proteins including silk fibroin can be modified by controlled structural change, which is regularly monitored by Fourier transform infrared spectroscopy (FTIR) by peak fitting of the amide I band. Currently there is no fixed methodology to compare and follow secondary structural differences without significant operator input leading to subjectivity and error.

This contribution establishes a method for such analyses to be carried at high levels of autonomy applicable to a wide range of proteins and the conformational changes have been quantified as a single energy change output, which clearly shows the progression of the annealing process used. We propose that the approach can help in the development of silk based materials for biomedical applications where tuning of the physical and mechanical properties of the silk are needed to guarantee optimum activity.
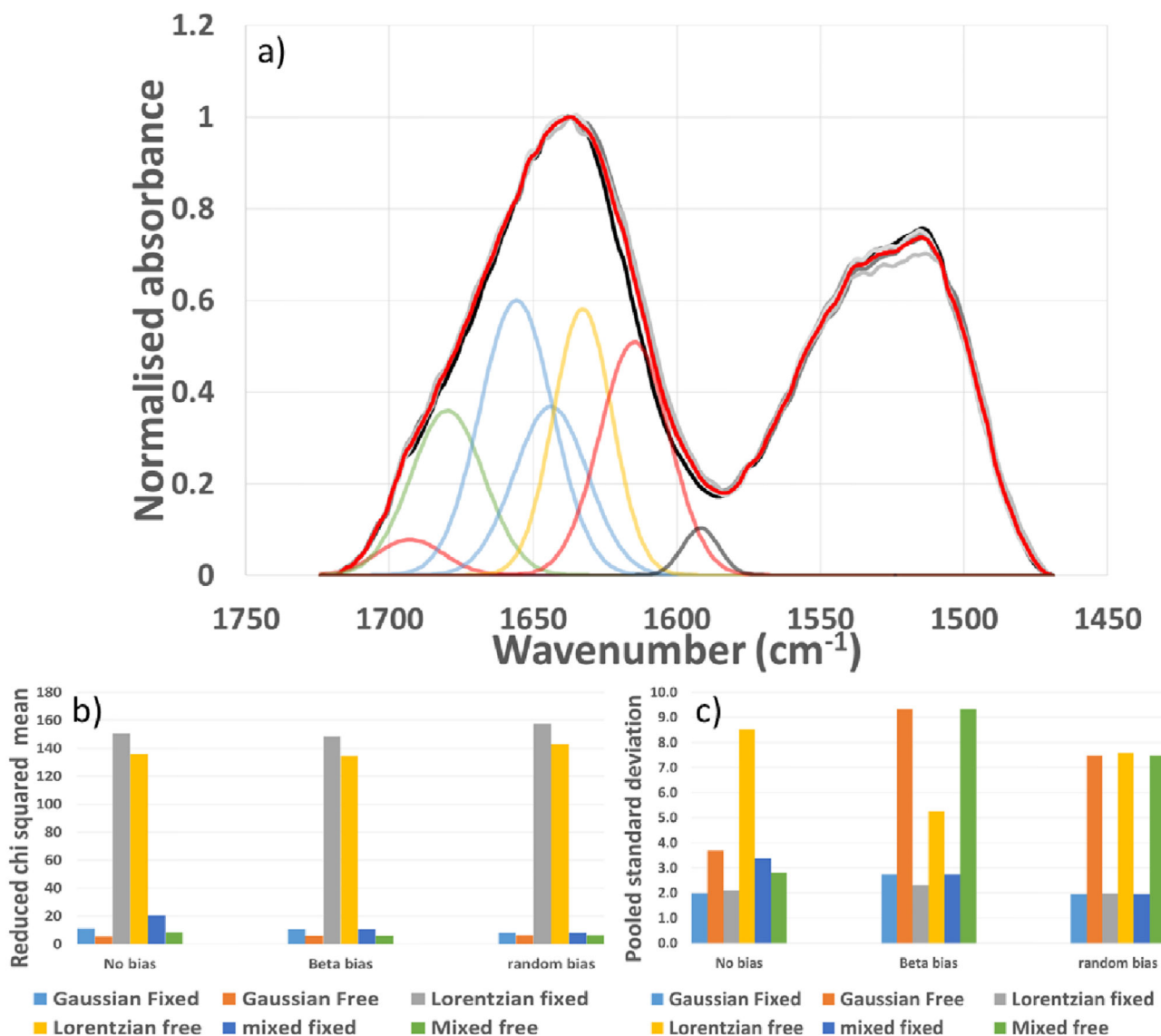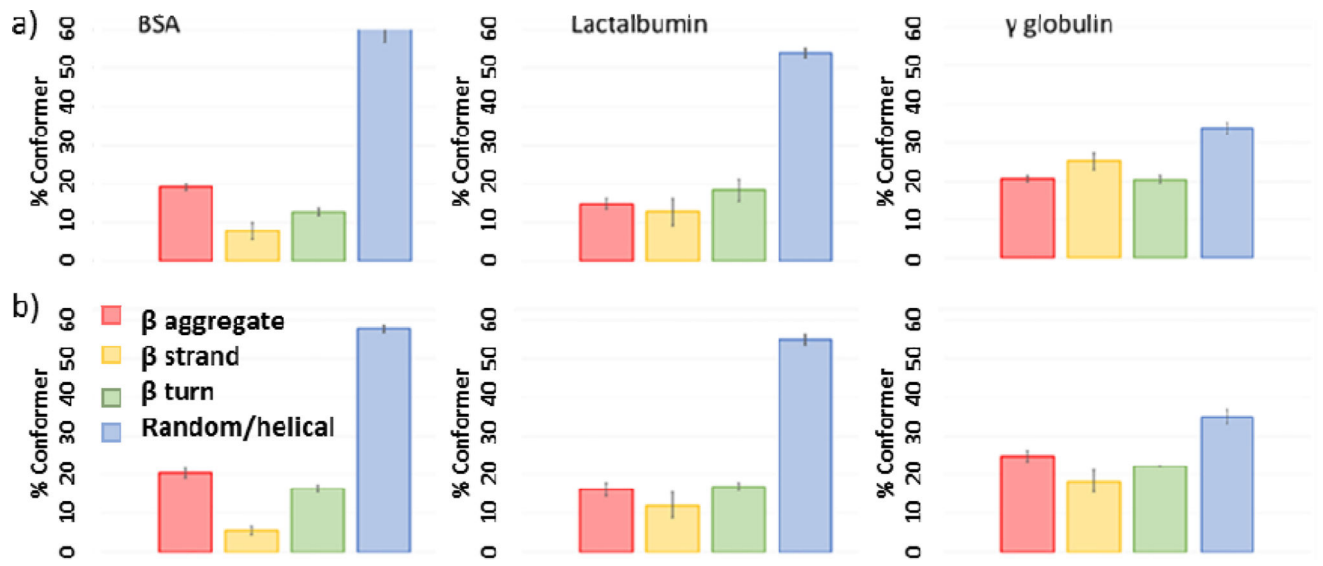
Figure 1.
FTIR-ATR of silk films a) Normalised spectra from 5 replicate (grey shades) non-annealed silk films and mean spectrum (red), and fitted conformers – (amide II fitting peaks have been omitted for clarity) refer to materials and methods section for individual peak ID. b) Reduced chi square from curve fitting and c) Pooled standard deviation of the fitted replicate non-annealed silk films for different distributions or combinations of the variables selected. Terms 'free' and 'fixed' refer to the level of freedom for the particular conformer maximum to move, 'free' is within literature ranges and 'fixed' is limited to the centre point of these ranges.
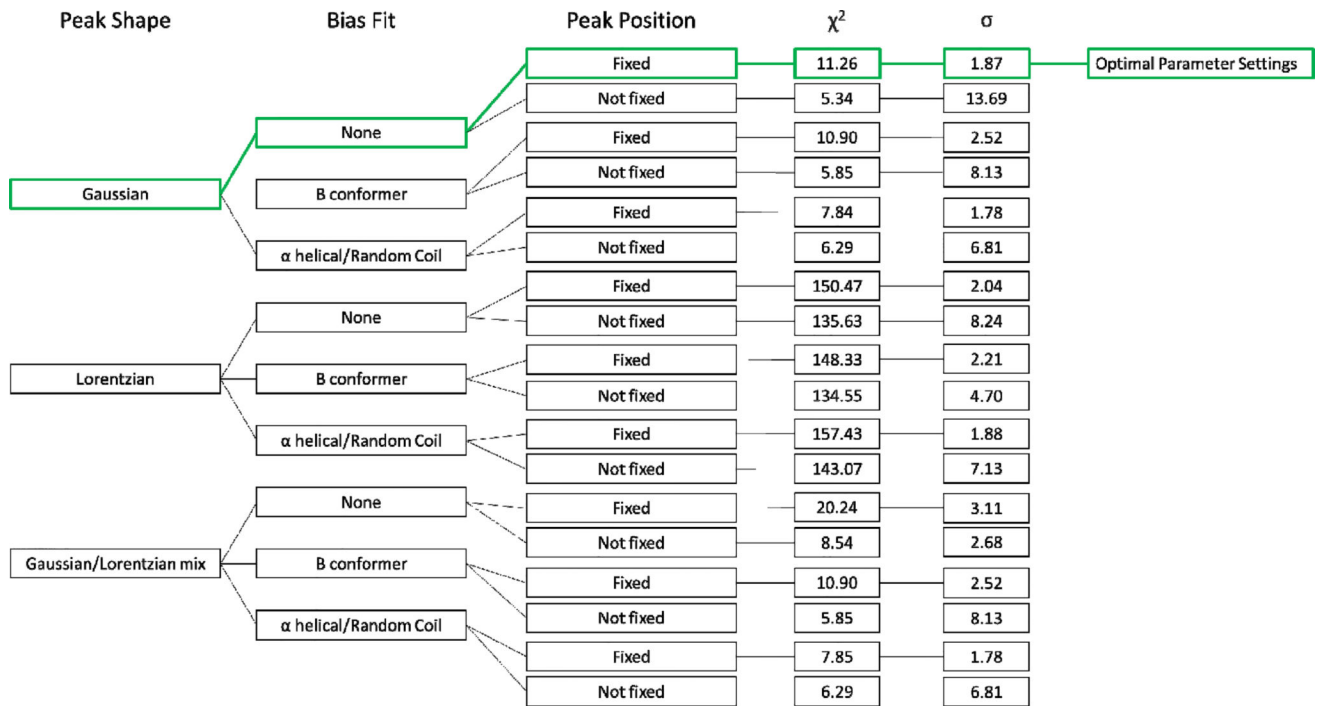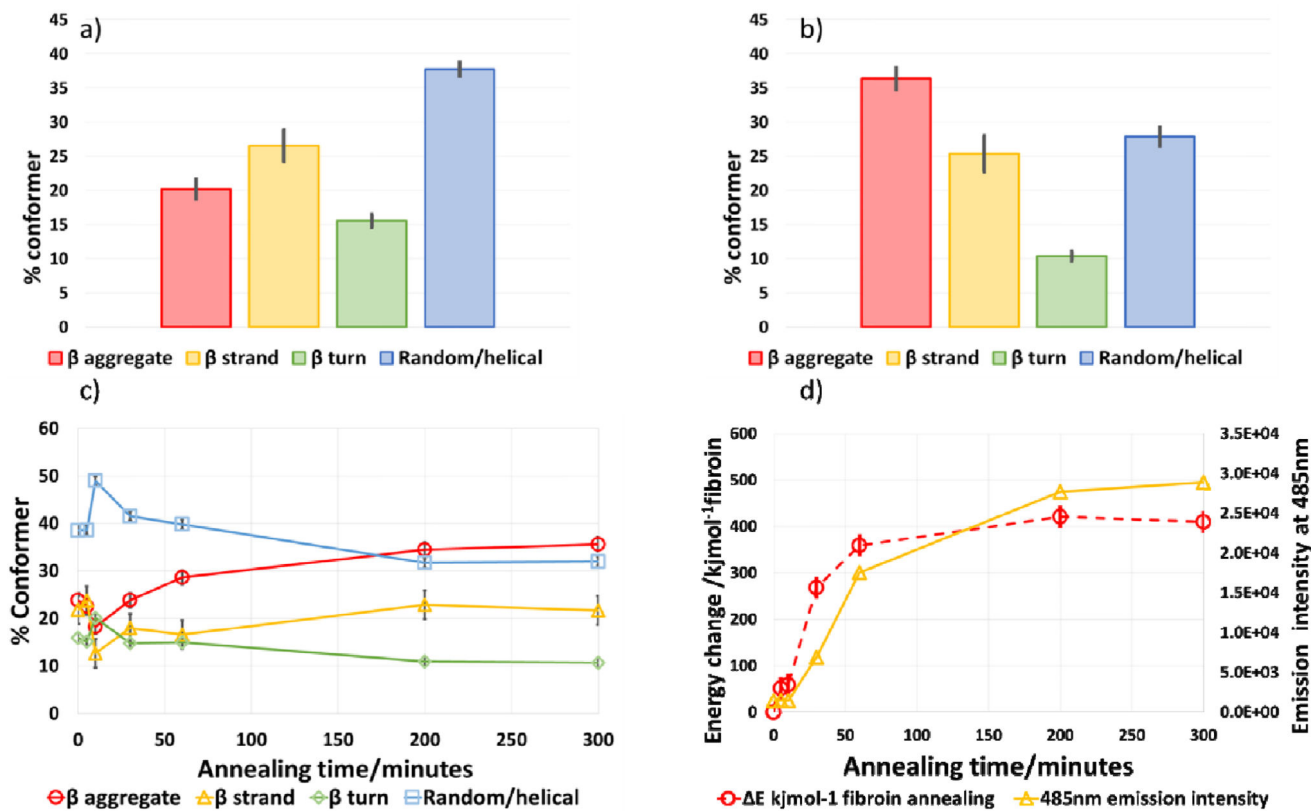
Figure 2.
Flow chart displaying all variable combinations considered in this study, the green route indicates the variables selected based on both chi squared and standard deviation values.
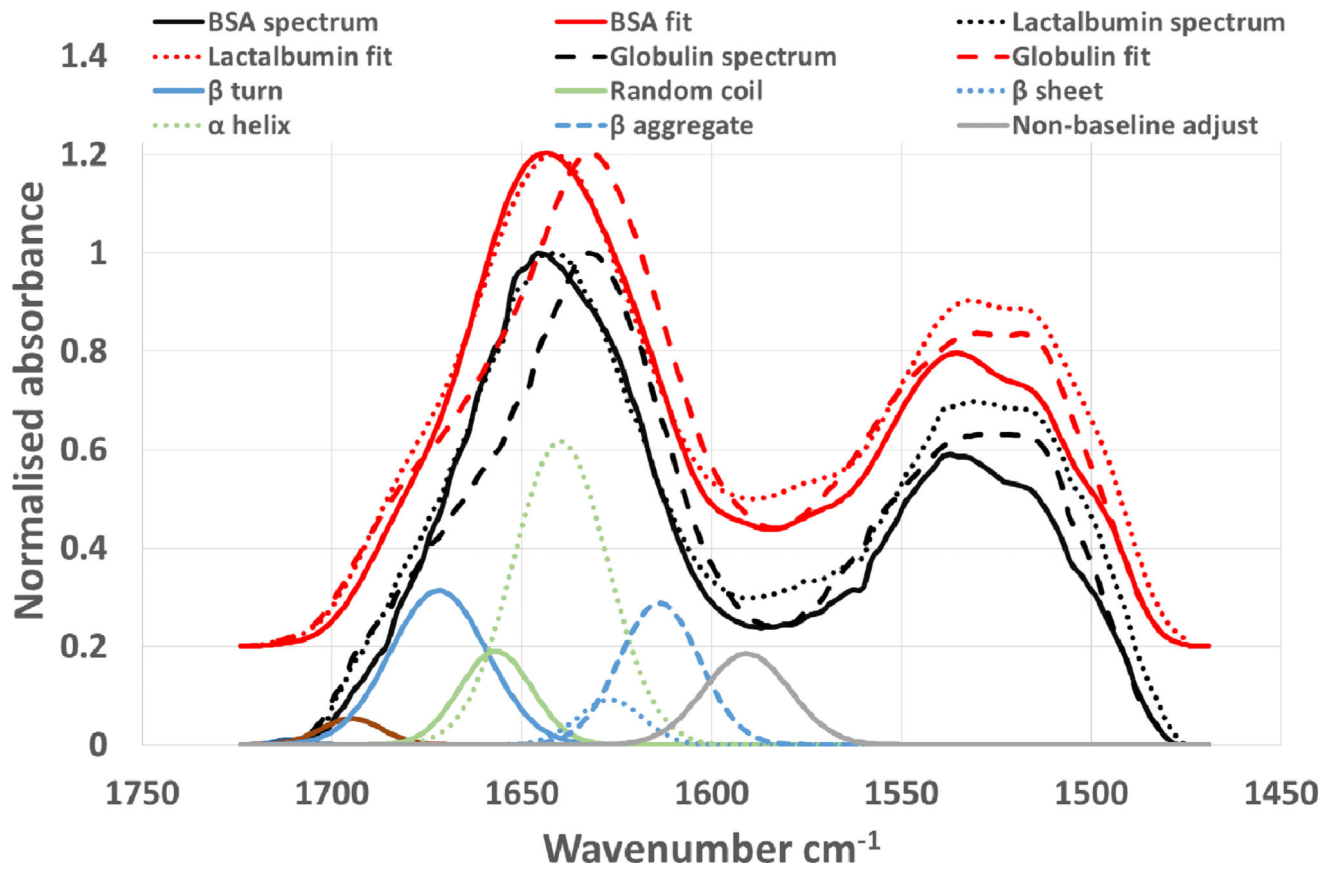
Figure 3.
Protein reference spectra and peak fitting (y offset 0.2)- (amide II fitting peaks have been omitted for clarity). The conformer spectral absorbances are from the α lactalbumin fitting. All spectra and fits are the average of 5 replicate analyses and fitting procedures.
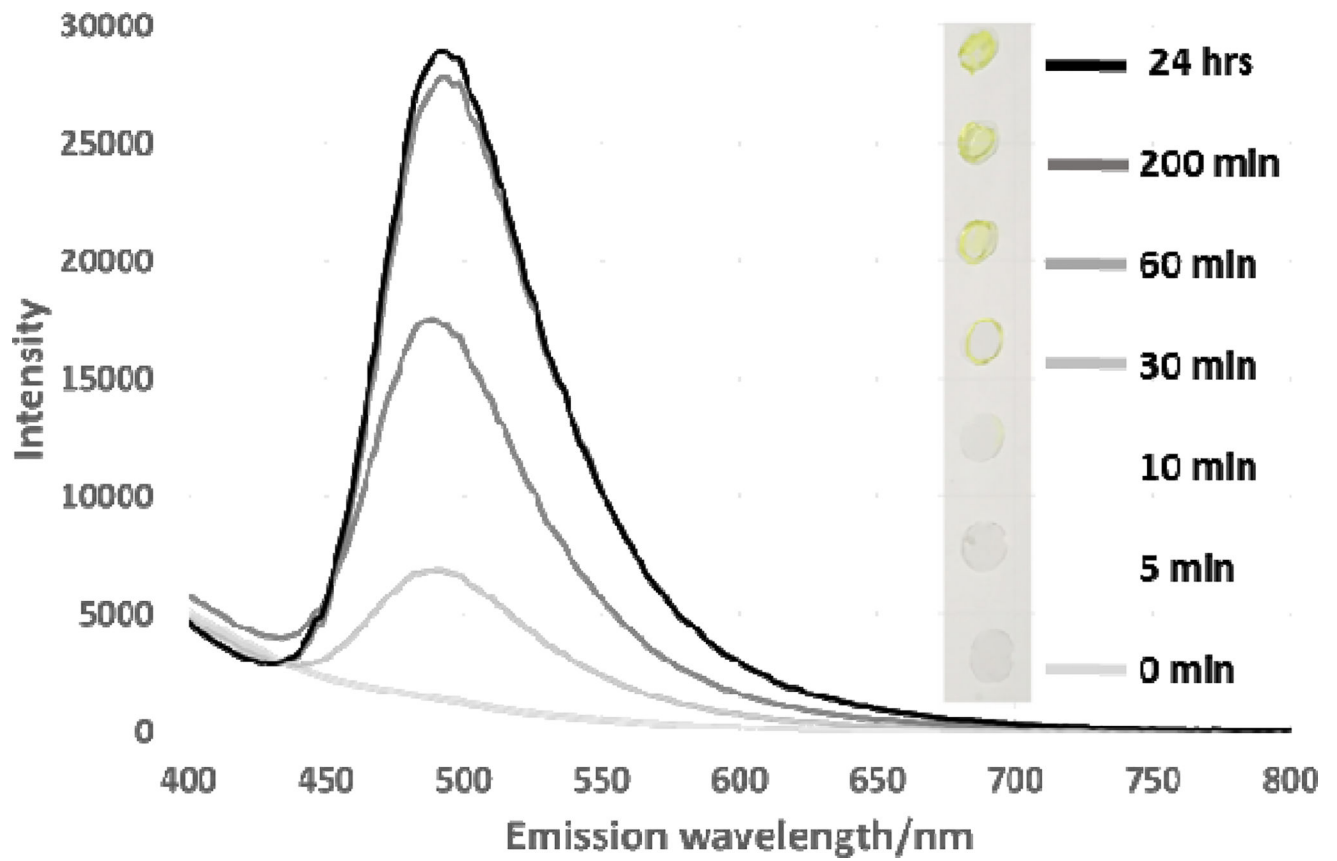
Figure 4.
Peak fitting data for 5 replicate samples of 'model' proteins: (a) powders as received, (b) freshly prepared films (from water on glass slides). Error bars show 1 sigma variance.

Figure 5.
Silk films: a) Conformer composition of un-annealed silk films, b) Conformer composition of annealed films after 24 hours; c) Conformer changes during the annealing process (χ_ν^2 and square root mean variance 9.3, 1.53 and 13.0, 1.72 pre and post annealing respectively), and d) energy changes and fluorescence (β aggregate content) during annealing. More detailed information on the changes occurring in the first 50 minutes of the annealing process are provided in the SI.

Figure 6.
Thioflavin T amyloid staining. Emission spectrum under 360 nm excitation and visible appearance under white light (annealing time shown in minutes). A lower wavelength to that routinely used for amyloid staining was used to avoid saturation of the detector.

Table 1

Comparison of quantitative data found in this study and by others using a range of quantitation methods.

Method	β content (%)	non β content (%)	References
FTIR-ATR	50–63	37–50	[This contribution]
X ray diffraction	64–68	32–36	[73]
^{13}C CP-MAS NMR	55–60	40–45	[67,74]
FTIR-ATR	53 – 70[*], 49	30 – 47[*], 51	[34[*], 75]

[*] Ranges found during annealing includes peaks from turn structures to compare directly with the methodology of this contribution.